A&A 478, L11–L14 (2008)
DOI: 10.1051/0004-6361:20078838
© ESO 2008

Astronomy & Astrophysics

Letter to the Editor

Doppler imaging an X-ray flare on the ultrafast rotator BO Mic

A contemporaneous multiwavelength study using XMM-Newton and VLT⋆,⋆⋆

U. Wolter[1], J. Robrade[1], J. H. M. M. Schmitt[1], and J. U. Ness[2]

[1] Hamburger Sternwarte, Gojenbergsweg 112, 21029 Hamburg, Germany
e-mail: [uwolter;jrobrade;jschmitt]@hs.uni-hamburg.de
[2] Arizona State Universtity, PO Box 871404, Tempe, AZ, 85287-1404, USA
e-mail: Jan-Uwe.Ness@asu.edu

Received 11 October 2007 / Accepted 21 November 2007

ABSTRACT

We present an analysis of contemporaneous photospheric, chromospheric and coronal structures on the highly active K-dwarf star BO Mic (Speedy Mic). We concentrate on a moderate flare that we localize in the stellar atmosphere and study its energetics, size and thermal behavior. The analysis is based on strictly simultaneous X-ray, UV- and optical observations carried out by XMM-Newton and the VLT. We use Doppler imaging and related methods for the localization of features. Based on X-ray spectroscopy we study the the coronal plasma in and outside the flare. The flare emits in X-rays and UV, but is not detected in white light; it is located at intermediate latitude between an extended spot group and the weakly spotted pole. We estimate its height to be below 0.4 stellar radii, making it clearly distinct in longitude and height from the prominences found about two stellar radii above the surface. In contrast to BO Mic's photospheric brightness, neither its chromospheric nor its X-ray emission show a pronounced rotational modulation.

Key words. stars: activity – stars: chromospheres – stars: coronae – stars: flare – stars: imaging – stars: individual: BO Mic

1. Introduction

The level of stellar activity is related to the efficiency of a star's dynamo, operated by an interplay of convection and rotation, with faster rotation resulting in higher activity for a given type of star (Schrijver & Zwaan 2000). Extreme activity phenomena are observed on the ultrafast rotating, highly active, young K-dwarf star BO Mic (K2V, $P_{\rm rot} = 0.380 \pm 0.004$ days, $v \sin i \approx 135\,{\rm km\,s^{-1}}$, $d = 44.5$ pc), nicknamed "Speedy Mic". BO Mic produced the largest X-ray flare observed during the ROSAT all-sky survey, with a peak flux of $\approx 9 \times 10^{31}$ erg/s in the ROSAT PSPC passband (0.1–2.4 keV, Kürster 1995). Follow-up observations of BO Mic showed its very high projected rotational velocity and short rotation period. Subsequent Doppler imaging studies revealed a richly spotted photosphere and reconfigurations of active regions during only a few stellar rotations (Wolter et al. 2005 = WSW 2005; Barnes 2005), making *strictly* simultaneous and coherent observations mandatory. We observed BO Mic during two consecutive nights on 2006 October 13/14 and 14/15 simultaneously with *XMM-Newton* and VLT/UVES at ESO Paranal. The observations were scheduled to maximize simultaneous and continuous visibility of the target by both instruments.

In this Letter we report the first results of our campaign, presenting a coherent "snapshot" of BO Mic's active regions that concentrates on the localization and analysis of a moderate flare.

⋆ Based on observations obtained at the ESO VLT Obs. No. 078.D-0865(A) and *XMM-Newton* Obs. Id. 0400460301 and 0400460401.

⋆⋆ Doppler imaging line profiles are only available in electronic form at http://www.aanda.org

2. Observations and data analysis

Our VLT/UVES observations lasted two half nights, $JD_0 + 0.49$ to 0.70 and $JD_0 + 1.48$ to 1.69 with $JD_0 = 2\,454\,022.0$. The *XMM-Newton* observations exceeded these time spans, lasting from from $JD_0 + 0.48$ to 0.79 and from $JD_0 + 1.47$ to 1.73. In total we obtained about 50 ks of X-ray data and 32 exposures of optical photometry from the optical monitor (OM) onboard *XMM-Newton*. Our 142 UVES spectra completely cover two semi-rotations of BO Mic with some phase overlap.

UVES was operated in dichroic mode, covering the spectral range 3260 to 9460 Å with a spectral resolution of $\lambda/\Delta\lambda \approx 40\,000$. UVES exposures lasted between 200 and 250 s, separated by the CCD readout time of 10 s. The spectra were reduced using the package REDUCE described in Piskunov & Valenti (2002). We carried out an approximate flux calibration using synthetic spectra from Hauschildt et al. (1999).

All *XMM-Newton* instruments obtained useful data of BO Mic; here we only present data gathered by the EPIC (European Photon Imaging Camera) and the OM (optical monitor). The OM was operated with the visual grism in the wavelength range 3000–7000 Å. Due to the brightness of BO Mic, the OM grism spectra are affected by coincidence loss, and we could not make use of either the full spectral resolution or of the absolute flux calibration, thus we had to restrict the analysis to relative spectrophotometry. All *XMM-Newton* data were reduced using the Science Analysis System (SAS) version 7.0 (Loiseau et al. 2006) with standard selection and filtering criteria. X-ray light curves are background subtracted, based on nearby source-free regions. Spectral analysis of the EPIC data was carried out with XSPEC version 11.3 (Arnaud 1996); for spectral fitting purposes we used a multi-temperature model,

Article published by EDP Sciences and available at http://www.aanda.org or http://dx.doi.org/10.1051/0004-6361:20078838

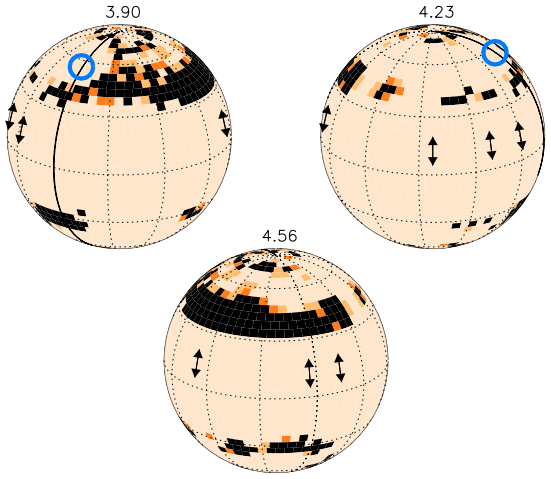

Fig. 1. Atmospheric structures of BO Mic reconstructed by Doppler imaging and related methods. All maps show the same features for the given rotation phases. Photospheric spot coverage is rendered as black, dark and light orange areas, representing 100%, 67% and 33% spot coverage, respectively. Equatorial arrows mark approximate longitudes of prominences observed in Ca K and H_α. The blue circle indicates the chromospheric emission region of the flare. Grid lines mark latitudes and longitudes in 30° steps.

assuming the emission spectrum of a collisionally ionized, optically thin gas as calculated with the APEC code (Smith et al. 2001) with abundances modeled once for the complete data set. To investigate spectral changes we then derived temperatures and volume emission measures ($EM = \int n_e n_H dV$) of the individual plasma components and calculated X-ray luminosities from the best fit models.

3. BO Mic's activity spatially resolved

3.1. Doppler images

The photospheric spots were reconstructed from the VLT spectroscopy using our Doppler imaging (DI) algorithm CLDI (WSW 2005) on a grid resolving 2020 surface elements. We adopted an inclination angle of 70° for the stellar rotation axis, $v \sin i = 134$ km s^{-1} as determined by WSW 2005 in agreement with Barnes (2005), and a rotation period of 0.380 days (Cutispoto et al. 1997). For DI, the spectra were added in pairs, resulting in 72 spectra with a typical S/N ratio of 400 at 6000 Å. The spectra cover 1.1 stellar rotations with a homogeneous phase sampling and a gap of two rotations between the observations of the two hemispheres. The line profiles used for the DI were obtained by a spectrum deconvolution of the wavelength range 6390–6440 Å (see WSW 2005 for details).

In Fig. 1 we show a reconstruction of BO Mic's active regions. The spots on the surface show a largely non-polar (similar to Barnes 2005, although at lower latitude), azimuthally quite asymmetric distribution, with spots both in the northern and southern hemispheres. The large-scale reliability of our Doppler image, at least in longitudinal spot distribution, is illustrated in Fig. 2, where we compare the observed light curve with that computed from our DI in the 6000–6500 Å range. The light curve supports the reality of the southern spots found in the DI. While their appearance in the DI depends on the adopted spot brightness, the reconstructions including southern spots yield a significantly better fit to the OM-light curve.

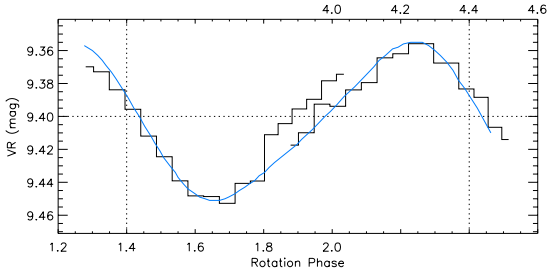

Fig. 2. BO Mic's photospheric emission as measured by *XMM-Newton's* optical monitor (black) and computed from our Doppler image (blue). The left and right sections of the black curve render the first (lower phase scale) and second (upper scale) observed semi-rotation, respectively. The emission is integrated from 6000 to 6500 Å, i.e. centered between Johnson-V and R. The estimated error is ±0.003 mag.

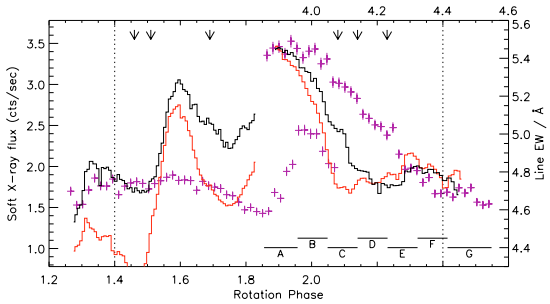

Fig. 3. BO Mic's coronal and chromospheric emission. Purple crosses show flux and 1σ-errors of the soft X-ray emission (0.2–5.0 keV) as registered by *XMM-Newton's* EPIC-pn detector. The black and red curves give the Ca K and H_α equivalent width, respectively. Arrows mark the phases of sub-observer passage for the prominences shown in Figs. 1 and 5. The horizontal lines "A–G" indicate bin intervals for the data points of Fig. 4. Phase annotations are the same as in Fig. 2.

Concerning the non-periodic components of the OM-light curve, we note that the peaks at phases 1.25 and 4.25 differ in brightness. This reflects a change in the spot pattern during the three rotations between them, as supported by changes in the corresponding photospheric line profiles.

3.2. The chromospheric and coronal perspective

In Fig. 3 we plot the temporal evolution of the chromospheric and coronal activity in terms of Ca K and H_α equivalent width and soft X-ray emission in the 0.2–5 keV energy band (crosses). Clearly, neither varies smoothly between the two nights. The X-ray light curve shows flares during both nights; the second night seems to consist of one coherent event with several bumps in the decaying X-ray light curve, suggesting reheating events.

To verify this interpretation we investigated the evolution of the X-ray emitting plasma in terms of emission measure and temperature. We divided the X-ray data into seven segments ("A–G" in Fig. 3) and performed a spectral analysis (cf. Sect. 2). The results are shown in Fig. 4: the temperature decreases with decreasing emission measure during the intervals A–D, which is consistent with the decay phase of a flare. During interval E the temperature rises, indicating additional energy input. The temperatures of 20–30 MK are typical for moderate flares.

Outside the flaring phases the X-ray light curve is relatively flat and apparently dominated by a stable quasi-quiescent level; it varies only by 20% peak to peak. As visible in Fig. 3, this modulation has a local maximum centered on phase $\phi \approx 1.55$, so it may be correlated with the photospheric brightness minimum

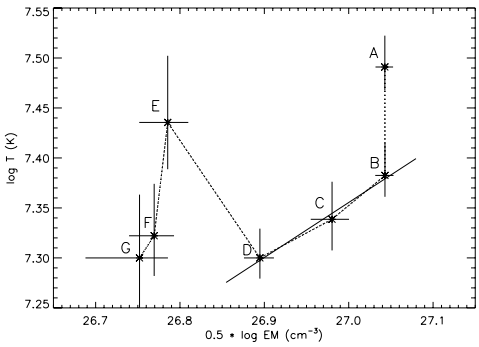

Fig. 4. Evolution of emission measure and temperature for the hot plasma component during the flaring, with 1σ errors as determind by the X-ray spectral fit. $EM^{0.5}$ is used as a proxy for the plasma density. The solid line shows a linear fit to points B–D, corresponding to the decay of the first flare event. Further energy release is evidenced by the deviation of points E–G from the decay path. The time bins of points "A–G" are given in Fig. 3.

at $\phi \approx 1.65$ (Fig. 2). However, based on one observed rotation, and in the presence of flaring, this remains speculative.

3.3. Localizing prominences and the flare

In Fig. 5 we provide a detailed view of the evolution of the Ca K emission line profile during our observations. Specifically, we show the time series of line profiles processed by an unsharp-masking filter that enhances fast changes in the core profile. The unsharp masking is performed by dividing the profile time series by a temporally smoothed copy of itself. For Fig. 5, wavelengths were transformed to velocity units, absorption dips in the profile are shown in blue while emission features are shown red. Several absorption features clearly move through the Ca K line profiles. In order to localize the corresponding prominences in longitude we fit pronounced deformations migrating redward through the core profiles with sine functions depending on rotation phase ϕ through

$$v_{\rm rad}(\phi) = v\ \sin i \cdot r/R_*\ \cos(\pi/2 - \theta)\ \sin(\varphi - 2\pi\phi) \qquad (1)$$

which describes the radial velocity of an atmospheric feature located at the radius r (divided by the stellar radius R_*), the latitude θ and longitude φ. Essentially, the phase of $v_{\rm rad} = 0$ determines the longitude while the slope $\frac{dv}{d\varphi}$ determines the height of a prominence when θ is adopted as the subobserver latitude. In this way we obtain the approximate longitudes and heights of six prominences marked in Fig. 5. These prominence parameters agree with those obtained by the same procedure from the H_α core profiles. Their radii range between 2.5 and 3.5 R_* with an uncertainty of $\pm 0.5\,R_*$, i.e. they are about 2 R_* above the surface. In Figs. 1 and 3 the approximate longitudes and phases of the structures causing absorption transients in the Hydrogen Balmer and Ca H and K lines are marked by arrows. Such fast-moving, often periodic line profile deformations can be attributed to "prominences", i.e. clouds of relatively cool material magnetically kept in co-rotation high above the stellar surface, and already observed on BO Mic (Collier Cameron et al. 2003; Dunstone et al. 2006). Given their rapid movement through the line profile, these prominences cannot be located close to the stellar surface. Only one pronounced deformation of the Ca K line core moves through the profile compatible with an emission feature close to the stellar surface. Shown in Fig. 5, it passes the profile center at phase $\phi = 4.0 \pm 0.02$. Using Eq. (1) to trace the emission peak through the line profile, we locate its

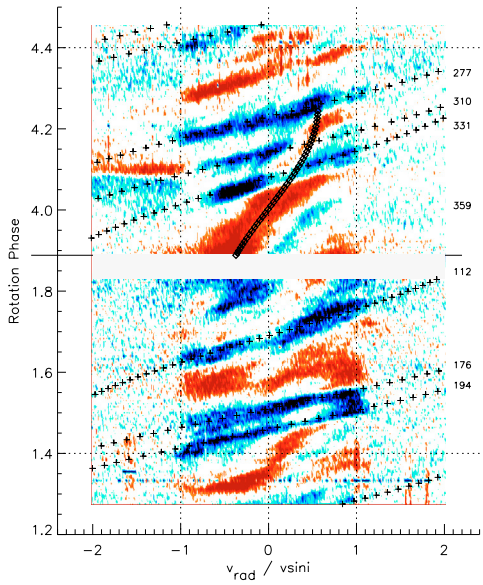

Fig. 5. Evolution of the Ca K emission: Ca K line core profiles, processed by unsharp masking are rendered as a function of wavelength (units of $v \sin i$) and rotation phase. Absorption dips in the profile appear blue while emission bumps are shown red. Plusses indicate sine-fits according to Eq. (1). They are used to localize absorbing prominences, their longitudes are given to the right. The fit to the flare-induced chromospheric emission is marked by diamonds. See text for discussion.

emitting region on the surface at a latitude of $\theta = 56 \pm 10°$ and a longitude of $\varphi = 359 \pm 10°$, marked by a circle in Fig. 1.

It should be noted that this "flare plage" could also be located at the same latitude south of the equator, since for each rotation phase the radial velocity is the same there as for the northern location. The same effect causes a north-south-ambiguity of features found in all Doppler images (e.g. Piskunov et al. 1990). However, in that case, the weak emission rise in H_α and Ca K at phase $\phi \approx 4.3$ (see Fig. 3) could not originate from the plage location because south of the equator this latitude is no longer visible. Thus, this feature is very likely located in the north. Since the enhanced Ca K and H_α emissions clearly coincide with the X-ray flare we are confident that the location marked in Fig. 1 is indeed the chromospheric footpoint of the X-ray flare.

4. The flare: evolution and energetics

Our contemporaneous optical and X-ray data allow us to further characterize the flaring plasma. Unfortunately, our observations did not cover the impulsive rise of the chromospheric and coronal flare emission and we see no flare signatures in the photometric lightcurves. However, a short increase prior to the peak of the X-ray emission is visible in Fig. 3, suggesting that our observations cover the very end of the rise phase of the flare and all of its decay. The decay to the "quiescent" level takes about 0.45 and 0.29 rotation phases or 4.1 and 2.6 h for the soft X-ray and Ca K emission, respectively. The H_α emission decays even faster, however, it is strongly influenced by the prominences.

Assuming that the flare occurs in a single plasma loop and using the method described in Reale et al. (2004), we estimate the flare loop size from the EM-T diagram shown in Fig. 4. Fitting the decay of the first heating event, the derived slope yields an upper limit of $l \lesssim 0.4\,R_*$ for the loop half length. This upper limit even remains valid if the flare occurred in an arcade of several loops, because in this case each individual loop would have to be smaller. While considerably larger than solar

coronal loops, this is much closer to the star than the prominences located at $h \approx 2\,R_*$ (cf. Sect. 3.3). Reheating occurs between rotation phases 4.2 and 4.3, indicating its connection to the sudden slight increase in X-rays seen in Fig. 3 at phase 4.25. This is possibly related to the increase in H_α and Ca K emission observed about 0.05 rotations (≈30 min.) later. The total emitted energy of the flare observed in soft X-rays, $\approx 1.3 \times 10^{34}$ erg in the 0.2–10 keV band, appears to originate predominantly, but not exclusively, from a single energy release. The peak luminosity of the flare in soft X-rays of $\approx 1.4 \times 10^{30}$ erg/s (6×10^{29} erg/s in the 1–8 Å GOES-band) is considerably larger than the maximum power in Ca K and H_α of $\approx 2.0 \times 10^{28}$ erg/s and $\approx 1.0 \times 10^{29}$ erg/s, respectively. This energetic mismatch of coronal and chromospheric emission would be unusual for a solar flare where these emissions – with considerable variations – tend to be comparable (Foukal 2004; Johns-Krull et al. 1997; Emslie et al. 2005).

5. Summary and discussion

We observed the highly active K-star BO Mic during one rotation with completely simultaneous coverage from soft X-ray to optical wavelengths. The observations were carried out in two blocks separated by two stellar rotations with all observed indicators of photospheric, chromospheric and coronal activity showing pronounced variations.

The Doppler image (DI) shows only a few spots near the visible pole. Most spots are asymmetrically distributed at mid-latitudes, leading to a roughly sinusoidally modulated photospheric light curve with a peak-to-peak amplitude of ≈0.1 mag. There are additional small non-periodic components in the optical light curve; in agreement with results of previous observations of BO Mic (WSW 2005), this indicates some reconfigurations of spots on rather short timescales of a few rotations.

The chromospheric light curves (H_α and Ca II) and coronal light curve (soft X-ray emission) are only weakly correlated with the photospheric modulation. The predominant variations of chromospheric emission are absorption transients in the H_α and Ca K line cores, which are caused by prominences about two stellar radii above the surface; their distribution is qualitatively similar to those analyzed for BO Mic by Dunstone et al. (2006). The longitudes of the prominences show no obvious connection to the photospheric spots. Whether the "quiescent" chromospheric emission is more intensive on the photospherically darker hemisphere, as suggested by our 2002 observations (Wolter & Schmitt 2005), cannot be reliably determined due to the strong prominence absorptions found here. Also, there is no clear evidence for X-ray absorption by these prominences, setting a strict upper limit to their column density.

The most conspicuous event during our observations was a flare lasting about 4 h; the flare is not registered in our broad band photometry, but shows up clearly in the H_α, Ca II and X-ray light curves. By tracing the radial velocity of its chromospheric emission in the Ca K line we localize the flare site in the stellar atmosphere. Somewhat surprisingly, the flare does not appear to be connected to the main concentration of activity in terms of dark spots; rather, it is located at the fringes of this region. As discussed in Sect. 3.3, this "flare plage" (which could also be a post-flare loop) could also be situated at the same latitude south of the equator, where the DI is only poorly defined due to poor visibility close to the stellar limb. At any rate, the "flare plage" is not associated with any distinguished feature of the photospheric spot pattern. Either such a spot feature is largely hidden by the southern limb or, more likely, it does not exist.

We determine the overall energetics and thermal evolution of the flare by simultaneously studying the soft X-ray emission. With a peak soft X-ray power of $\approx 10^{30}$ erg/s, this flare is a hundred times more energetic than a large solar flare in terms of peak flux and total radiated energy (Golub & Pasachoff 1997), however, it is still at least two orders of magnitude weaker than the largest flares observed on BO Mic. Assuming $\approx 10^{30}$ erg/s as an upper limit to the power radiated in the optical continuum, this would correspond to $\sim 10^{-3}$ of BO Mics total luminosity (WSW 2005), i.e. below the sensitivity of our photometry and consistent with the photometric non-detection.

In addition to the large flare, BO Mic's soft X-ray emission exhibits another, smaller flaring event and possibly a slow modulation with ≈20% peak to peak amplitude. The slow modulation may be correlated with the observed photospheric spot distribution; however, due to the flares and only one observed rotation, this remains inconclusive. Also, no optical spectra are available for the first flare, therefore it could not be localized. However, both X-ray flares appeared at similar rotation phases ($\phi \approx 2.0$ and 4.0), i.e., the first flare was situated on the same hemisphere as the second or sufficiently close to one of the poles. Qualitatively, our X-ray lightcurve is similar to that observed by Hussain et al. (2007) for the ultrafast rotating K-star AB Dor. Also, our value for the coronal flare loop height of $\lesssim 0.4\,R_*$ is compatible with their height estimate of coronal structures, once more confirming the similarity of AB Dor and BO Mic.

To our knowledge, the flare on BO Mic is the first X-ray flare that could be localized on a Doppler image. Interestingly, the flare occurs on a rather inconspicuous portion of the atmosphere as judged from the image. Extended observations of flaring events on a given star could reveal the spatial distribution of flare emerging sites. Physically, one expects flaring events to be associated with magnetic null lines. Since our UVES spectra are non-polarimetric, we cannot assess the location of magnetic null lines on BO Mic's surface. Clearly, a Zeeman Doppler image would be helpful to prove the association of stellar flare sites with magnetic null lines as expected from the solar analogy.

Acknowledgements. J.R. and U.W. acknowledge DLR support (50OR0105).

References

Arnaud, K. A. 1996, in Astronomical Data Analysis Software and Systems V, ed. G. H. Jacoby, & J. Barnes, ASP Conf. Ser., 101, 17
Barnes, J. R. 2005, MNRAS, 364, 137
Collier Cameron, A. C., Jardine, M., Wood, K., & Donati, J.-F. 2003, EAS Publ. Ser., 9, 217
Cutispoto, G., Kurster, M., Pagano, I., & Rodono, M. 1997, Inf. Bull. Var. Stars, 4419, 1
Dunstone, N. J., Barnes, J. R., Cameron, A. C., & Jardine, M. 2006, MNRAS, 365, 530
Emslie, A. G., et al. 2004, J. Geophys. Res., A110, 11103
Johns-Krull, C. M., Hawley, S., Basri, G., & Valenti, J. A. 1997, ApJS, 112, 221
Foukal, P. 2004, Solar Astrophysics (New York: Wiley)
Golub, L., & Pasachoff, J. M. 1997, The solar corona (Cambridge University Press)
Hauschildt, P., Allard, F., & Baron, E. 1999, ApJ, 512, 377
Hussain, G. A. J., Jardine, M., Donati, J.-F., et al. 2007, MNRAS, 377, 1488
Kürster, M. 1995, Flares and Flashes, IAU Coll., 151, 423
Loiseau, N., Ehle, M., Pollock, A., et al. 2006
Maggio, A., Pallavicini, R., Reale, F., & Tagliaferri, G. 2000, A&A, 356, 627
Reale, F., Güdel, M., Peres, G., & Audard, M. 2004, A&A, 416, 733
Piskunov, N., & Valenti, J. A. 2002, A&A, 385, 1095
Piskunov, N., Tuominen, I., & Vilhu, O. 1990, A&A, 230, 363
Schrijver, C. J., & Zwaan, C. 2000, Solar and Stellar Magnetic Activity (CUP)
Smith, R. K., Brickhouse, N. S., Liedahl, D. A., & Raymond, J. C. 2001, ApJ, 556, L91
Wolter, U., & Schmitt, J. H. M. M. 2005, A&A, 435, L21
Wolter, U., Schmitt, J. H. M. M., & van Wyk, F. 2005, A&A, 435, 261

Online Material

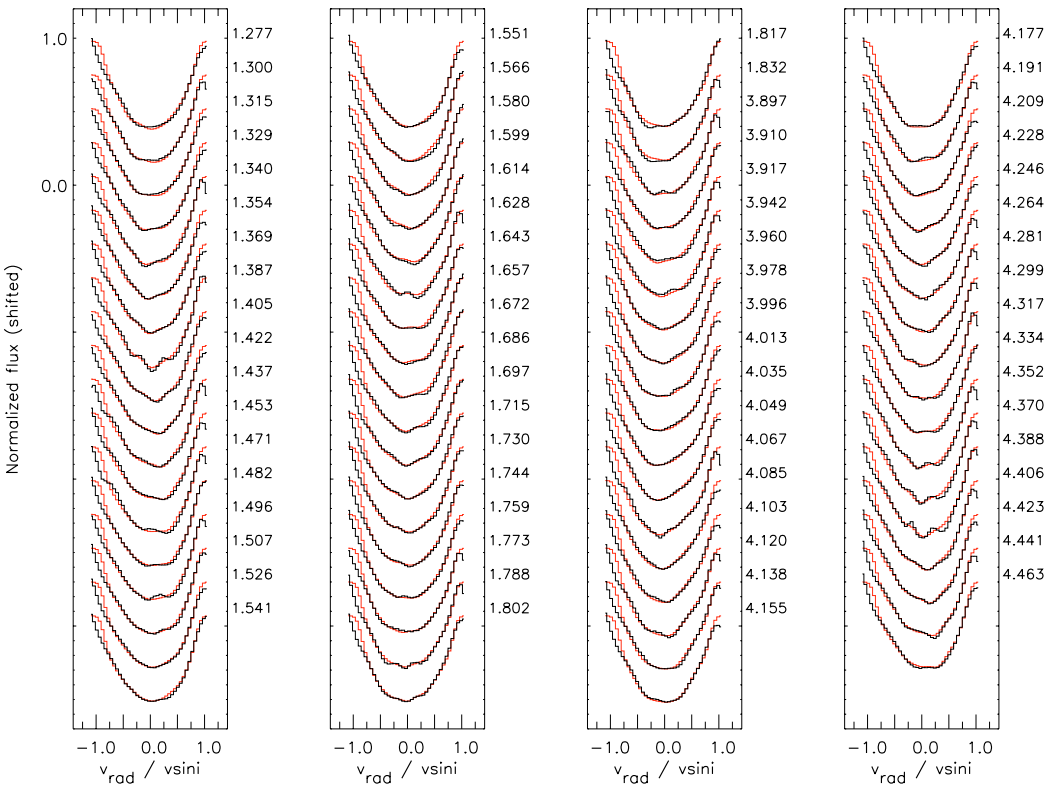

Line profiles of BO Mic, extracted by spectrum deconvolution in the range 6390–6440 Å (black) and fitted by Doppler imaging (red). Rotation phases are given to the right of each profile. Subsequent profiles of the time series are shifted, the flux scale is valid for the topmost profile of each column. Notice the phase overlap around phases 1.4 and 4.4 with a largely proper fit during both rotations. Unfortunately, between phases 1.8 and 3.9 there is no phase overlap. However, we attribute the slightly poorer fit in this phase range to a change of the spot pattern in the sub-observer region between the two different stellar rotations.